Japanese Journal of Applied Physics

PROGRESS REVIEW

Green VCSELs based on nitride semiconductors

Japanese Journal of Applied Physics **59**, SO0803 (2020) **PROGRESS REVIEW**
https://doi.org/**10.35848/1347-4065/ab9488**

Green VCSELs based on nitride semiconductors

H. Xu[1], Y. Mei[1], R. B. Xu[1], L. Y. Ying[1*], X. L. Su[1], J. P. Liu[2], and B. P. Zhang[1*]

[1]*Department of Electronic Engineering, Laboratory of Micro-Nano Optoelectronics, School of Electronic Science and Engineering, Xiamen University, Xiamen 361005, People's Republic of China*
[2]*Suzhou Institute of Nano-tech and Nano-bionics, Chinese Academy of Sciences, Suzhou 215123, People's Republic of China*

[*]E-mail: lyying@xmu.edu.cn; bzhang@xmu. edu. cn

Received January 14, 2020; revised April 21, 2020; accepted May 18, 2020; published online June 4, 2020

Vertical-cavity surface-emitting lasers (VCSELs) are promising in various applications including full-color mobile projectors, laser precision processing, display, armarium and high-speed air–water optical wireless communication systems with a unique combination of advantages. However, GaN-based VCSELs with emission wavelengths in green are challenging because of the low emission efficiency of green emitting InGaN QWs. This is known as the "green gap", which is mainly caused by the quantum-confined Stark effect and the high density of defects and dislocations. In this paper, we would like to discuss the origin of the "green gap" and possible approaches to overcome it, and then review our recent progress in green VCSELs: (1) lasing from 479.6 to 565.7 nm by using QD active area; (2) lasing at 545 nm by using QD-in-QW active structure; (3) lasing at 493 nm by utilizing blue-emitting InGaN QWs with the combination of cavity effect.

1. Introduction

Green lasers have attracted a lot of attention for use in numerous promising applications. Armarium[1–5] is one such application, used in prostate surgery to removing prostatic tissue.[1] 532 nm laser light can eliminate prostatic tissue which can highly and selectively absorb the laser and can result in thermal energy. This can release tissue and vapor bubbles to disrupt the cellular matrix, which is the so-called green light photo-selective vaporization of the prostate (green light PVP).[5] Green laser can also reduce bleeding volume and blood transfusions significantly in surgery.[6] The high-speed air–water optical wireless communication system is another important application of green laser owing to its low transmission loss, high modulation bandwidth, high security, high flexibility, low power consumption and low latency.[7–10] In addition, green lasers can also be applied in full-color mobile projectors,[11] laser precision processing,[12,13] and display.[14,15]

Green laser can be obtained in two ways: directly emitting from semiconductor laser diodes (LDs) based on InGaN,[11,16–26] AlInGaP[27,28] or perovskite[29–32] materials and wavelength conversion through a nonlinear optical process such as second harmonic generation (SHG).[28] Semiconductor LDs are characterized by smaller size and more stable performance compared to SHG lasers, although SHG technologies have been put to practical use in the green region.[23] In the semiconductor field, AlInGaP materials are not suitable for wavelengths shorter than 570 nm since the direct-indirect bandgap transition when the aluminum molar concentration rises up to 53%.[33] And perovskite lasers are still being developed and only optical pumped ones have been reported.[29] The InGaN-based semiconductors have the potential capacity for light emission in green light on account of adjustable direct bandgap energy of $In_XGa_{1-X}N$ (0.7–3.5 eV). Significant progresses have been made in the development of nitride lasers emitting green lights,[11,16–26] including edge emitting lasers (EELs)[21–26] and vertical cavity surface-emitting lasers (VCSELs).[11,16–20] The latter offers several advantages over EELs with *L–I* characteristics of low lasing threshold, small beam divergence, single longitudinal mode operation and circular beam shape.[16] Recently, great progress has been achieved in the field of green VCSELs with InGaN active area.[11,16,18–20,34] In 2008, our group firstly realized the optical pumping of blue-green GaN-based VCSEL after optimising the growth of InGaN/GaN QWs.[16] A lasing wavelength of 498.8 nm with a linewidth of 0.15 nm was observed under optical pumping at room temperature (RT). In 2016, we obtained continuous-wave (CW) lasing of current injected InGaN quantum dot (QD) VCSELs at 560.4 nm with a low threshold of 0.61 mA at RT for the first time.[18] In 2017, the lasing wavelength extended from 479.6 nm (blue-green) to 565.7 nm (yellow-green), covering most of the "green gap".[19] The same year, we achieved current injected GaN-based VCSELs lasing simultaneously in blue and green at RT by using a quantum dot in quantum well (QD-in-QW) active region. Lasing was first achieved at 545 nm with a threshold current of ~2 μA, and with a further increase of current, another lasing peak at 430 nm came out with a threshold current of ~5 mA.[20] In 2018, we fabricated green GaN-based VCSELs by combining normally blue-emitting InGaN/GaN QWs with a microcavity. Due to the cavity-resonant effect, the emission efficiency of localized states was strongly enhanced and, under higher injections, lasing was achieved in the nearly green (peak at ~493 nm), which presents novel opportunities for the design and fabrication of green VCSELs.[11]

Here, we will discuss the evolution of green VCSELs based on InGaN materials. We will primarily focus on recent key technological developments of GaN-based VCSELs, especially in the green region, and go in-depth on the physical principles. This manuscript will summarize the difficulties and challenges for fabricating high-performance green GaN-based VCSELs. After discussion of the "green gap" in Sect. 2, we will expatiate our experience to overcome manufacturing and material difficulties in Sects. 3–5. In Sect. 6, summary is given.

2. The "green gap" and possible approaches to overcome

The "Green Gap" is used to represent the low emission efficiency in the green spectral region, typically 500– 600 nm.[35] Compared with blue region, a higher indium content is necessary in InGaN in order to reach green light. This leads to a large strain in InGaN

layers when grown on GaN. As a result, large piezoelectric field and more defects are inevitable in case of InGaN/GaN QWs. The piezoelectric field causes band inclination, leading to the reduction of the electron–hole wavefunction overlap, and hence the reduction of radiative recombination,[36–38] which is the well know quantum-confined Stark effect (QCSE). On the other hand, defects will also capture carriers in the QW and reduce the emission efficiency. These will of course limit the performance of green emitting LDs. In the green region, because of the existence of defects and piezoelectric field caused by lattice mismatch, the emission efficiency of InGaN/GaN QWs decreases significantly.[39,40] And corresponding devices show strong efficiency droop[40–42] at high operating currents. This is the so-called "green gap." It of course will limit the performance of green emitting LDs. One of the fundamental issues that prevents longer wavelength LEDs is the big lattice -mismatch between InGaN and GaN resulting in strain-induced piezoelectric fields across InGaN/GaN quantum well structures and the crystal quality deterioration with phase separation of InN.[43] Simultaneously, increased In content gives rise to the QCSE, leading to reduction of the electron–hole wavefunction overlap, and hence the rate of radiative recombination.[36–38] The researchers came up with various promising approaches[22,44–49] to overcome these problems, including using InGaN–GaNAs QW structure which allows large electron–hole wavefunction overlap by confining the hole wavefunction in the GaNAs layer of the QW.[43] Others made effects in optimizing growth conditions of InGaN layer, such as employing triangular QWs to provide higher electron–hole wavefunction overlap,[46] additional process of indium pre-deposition before InGaN well layer growth,[47] introducing multiple interruptions during the InGaN-QW growth[48] and two-step high-temperature QW growth with AlGaN interlayers.[49] One effective way is to grow InGaN/GaN heterostructures along a semi- or non-polar direction to reduce or eliminate the internal electric fields.[22] The electric fields in *a*-plane (non-polar facet $11\bar{2}0$) and *m*-plane(facet $10\bar{1}0$) are vanished completely, in contrast to *c*-plane (polar facet 0001). Crystal planes orientated between polar and non-polar facets are called "semi-polar" planes, such as facet($20\bar{2}1$), facet($11\bar{2}1$). Compared with green EELs grown on *C*-plane GaN substrates,[21,50] semi- or non-polar GaN-based green EELs demonstrate better performance.[23–26] However, growing on free-standing semi-/non-polar GaN substrates is limited in a typical size of $10 \times 10\,\mathrm{mm}^2$ and extremely expensive. VCSELs are particularly worthy of academic investigation combining more unique features but more challenges. Up to now, RT pulsed lasing at 503 nm has been reported based on *c*-plane InGaN/GaN QWs. By adopting *c*-plane QDs, on the other hand, RT CW lasing up to yellow/green has been achieved. Nearly green VCSELs was also achieved by employing cavity-enhanced radiative emission of the localized states in a blue-emitting QWs.

3. Green VCSELs based on InGaN QDs

3.1. Advantages of QDs

InGaN/GaN QW structure is subjected to QCSE, defects and phase separation of InN, compared with GaAs materials, the large effective mass of the carriers in the GaN-based material system resulting in a higher transparent carrier density is another restriction on high-performance green lasers with InGaN QWs. In view of this, QDs instead of QWs are promising. QDs are three-dimensionally (3D) confined quantum structures with a δ-function-like density of states,[51] which leading to low lasing thresholds.[52] The stronger carrier localization effects in QDs s suppress lateral carrier diffusion and nonradiative recombination by impeding carriers from being captured by defects outside the QDs when compared to QWs,[53] in spite of the high dislocation densities in the material.[54] The formation of QDs is driven by the strain itself, and the strain remaining in the QD can be significantly reduced compared with the case of a two-dimensional QW epitaxial layer.[55]

Based on the above properties, lasers with QDs embedded in the active layer show more prominent performance, which surpassing QW lasers, such as the lower threshold current,[52,56] suppression of temperature dependence,[57] smaller linewidth enhancement factor[58,59] and higher material and differential gain.[60] Moreover, the dependences of energy band on QD's size and composition provide alternative approaches to adjust the emission wavelength,[61] indicating the potential to fabricate VCSELs emitting in the "green gap" by employing InGaN QDs as active region.

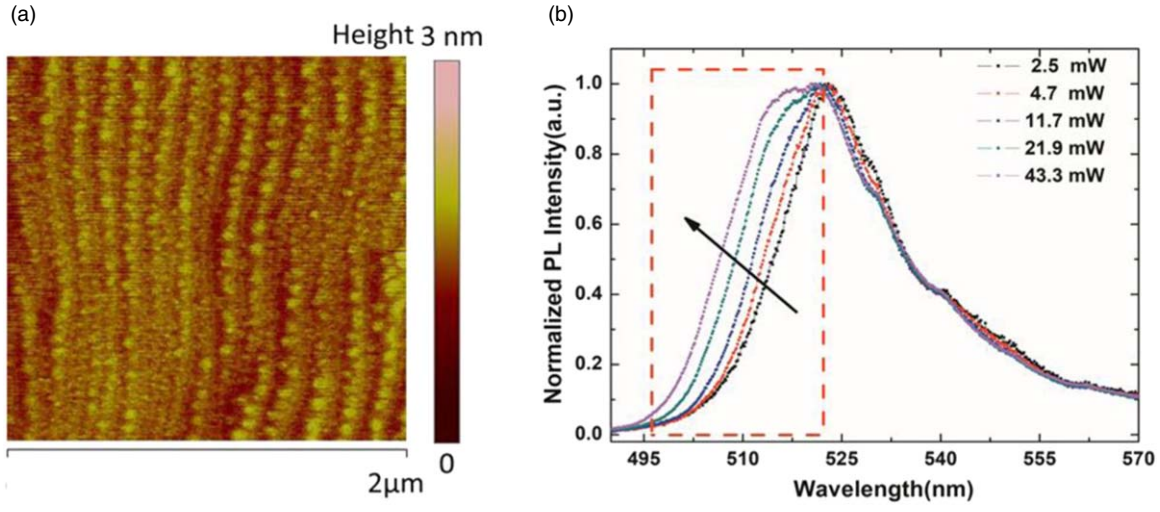

Fig. 1. (Color online) (a) AFM image of the uncapped InGaN QDs. (b) Low temperature normalized power dependent PL spectra of a QD wafer.

3.2. Image and emission properties of InGaN QDs

The InGaN self-assembled QD wafer used in this work was epitaxially grown on a *c*-plane sapphire substrate by a MOCVD system,[62] initialized by a 30 nm thick nucleation layer and then followed grew ordinally undoped GaN, n-type GaN, two layers of InGaN/GaN QDs, p-type AlGaN electron blocking layer, and p-type GaN. The GaN cap layers employed a two-step method to protect QD from decomposition during subsequent temperature ramping process to grow GaN barrier layer. The indium content of the QDs is about 27%. Detailed growth procedures are available in Ref. 62. Figure 1(a) shows the atomic force microscope (AFM) image of the uncapped InGaN QDs. The surface density of InGaN QDs is about $1.5 \times 10^{10}\,\mathrm{cm}^{-2}$, and the average diameter and height measured by AFM are 70 nm and 1 nm, respectively. Figure 1(b) shows the normalized photoluminescence (PL) spectra of the QD wafer under different excitation power at 5 K, excited by a 405 nm LD. The PL emission spectrum centered at around 520 nm. With increasing pump level, the PL spectra exhibit a slight blue shift at the shorter wavelength side due to band-filling effect, indicating that the QCSE in the QD wafer is very weak, which will enhance the overlap of electron and hole wave functions and allows higher internal quantum efficiency. Temperature dependent PL measurement (not given here) shows that the QD wafer used in this work has a large localization energy of 105.9 meV, which effectively prevents carriers' trapping at nonradiative centres and results in a high internal quantum efficiency of 41.1%.[63]

3.3. Fabrication process and properties of QD green VCSELs

The cross section of the fabricated GaN-based VCSEL is schematically shown in Fig. 2(a). The active region consisted of two periods of InGaN/GaN QD layers, sandwiched between p- and n-type nitride semiconductor materials. To form the cavity, we adopted two dielectric high reflectivity DBR mirror, a 12.5-pair TiO_2/SiO_2 bottom DBR and a 11.5-pair TiO_2/SiO_2 top DBR. The detailed fabrication process can be found in our previous reports. We first deposited SiO_2 patterned current confinement aperture (10 μm in diameter) and subsequently deposited indium tin oxide (ITO) current spreading layer, followed by a p-side contact around the current aperture and bottom DBR. Then a phase-shift adjustment TiO_2 layer before the formation of bottom DBR was deposited to minimize the absorption loss of ITO layer and increase the coupling of photons and carriers. Subsequently, the wafer was flip chip mounted on a copper suspending plate and then we utilized laser lift-off to remove the sapphire substrate and inductively coupled plasma (ICP) etching and chemical mechanical polishing (CMP) to remove the u-GaN layer with high dislocation density and flatted the surface. Finally, after an n-type contact and a top DBR depositing, we completed the device fabrication process. Photos of the fabricated single device, as well as the VCSEL array are shown in Figs. 2(b) and 2(c), respectively.

Figures 3(a) and 3(b) show the RT CW lasing spectra and light output-current–voltage (*L–I–V*) curves of a QD VCSEL, respectively. Single longitudinal mode lasing was observed at 560.4 nm with a spectrometer resolution limited FWHM of 0.16 nm, reaching to yellow-green region. The threshold current density was approximately 0.78 kA cm^{-2}, corresponding to the threshold current of 0.61 mA, lower than that of any InGaN QW VCSEL ever reported, whether violet, blue or green. The spectral longitudinal mode spacing between the adjacent cavity modes is about 24 nm, corresponding to a cavity length of 2.6 μm. By keeping the layer thickness above the active layer to be $(2n+1)/4 \cdot \lambda$, the active layer will be placed approximately on the antinode position of the standing wave. It will result in less absorption loss in the active region. On the other hand, such a thicker cavity length can avoid the sample damage caused by ICP. Such a long cavity leads to more than one cavity modes. Since the gain spectrum is also broad, it becomes easier to get resonance between the active layer and certain cavity modes. Due to the inhomogeneity in the QD size and the fluctuation of the In content, QD wafer exhibited a broad emission PL spectrum. Figure 3(c) shows the lasing spectra obtained from different VCSELs made from the same quantum dot wafer. With different cavity lengths obtained by CMP, the lasing wavelength extends from 479.6 to 565.7 nm, covering a substantial part of the "green gap".[19] The lasing wavelength of 565.7 nm was the longest ever reported for GaN-based VCSELs. It is worth noting that this wavelength is near the edge of the PL emission band. The gain should be not so high there but the strong coupling between electrons and photons can get over it. In another words, the large overlap between the active region and the anti-nodes of the optical field of the

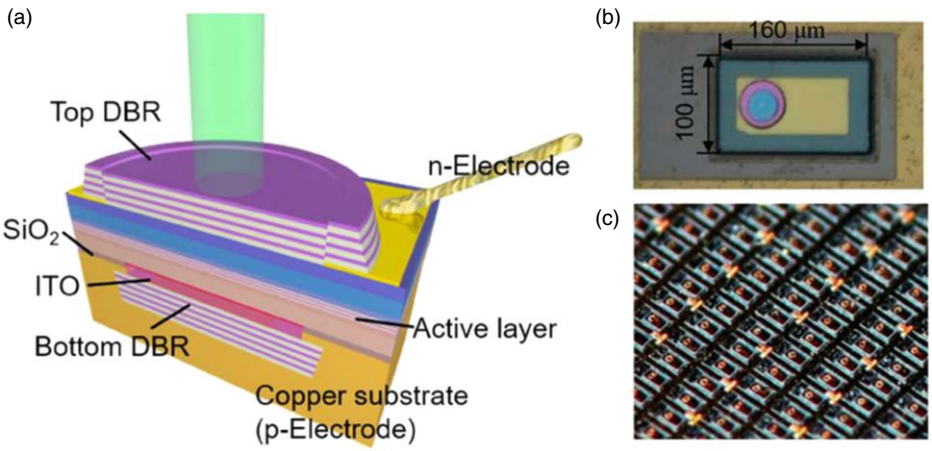

Fig. 2. (Color online) (a) Schematic structure of the green emitting VCSEL. (b) Photo of a single device. (c) Photo of the fabricated VCSEL array.

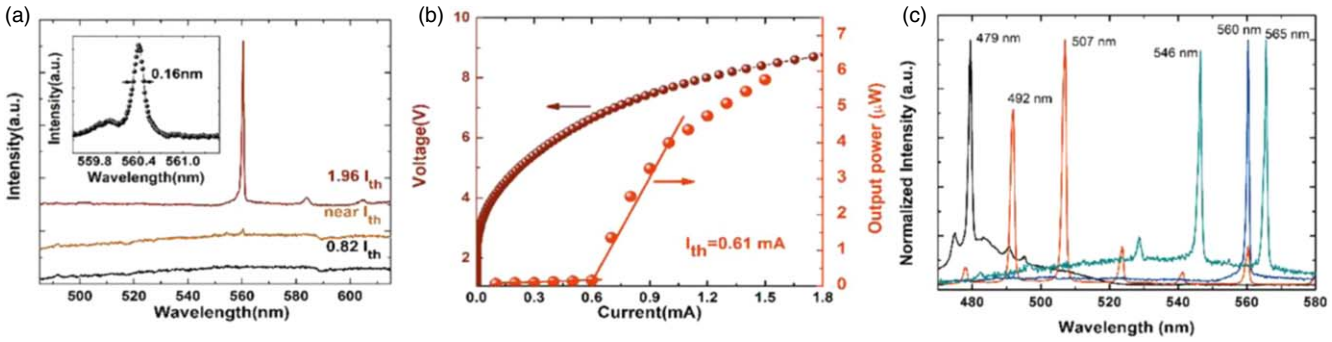

Fig. 3. (Color online) (a) Lasing spectra of the QD VCSEL emitting at 560.4 nm. (b) *L–I–V* curve of the QD VCSEL. (c) Lasing spectra obtained from different VCSELs made from the same QD wafer. The lasing wavelengths are from 479.6 to 565.7 nm.

standing-wave pattern in the cavity can effectively decrease the threshold gain of the VCSEL.

Low threshold RT CW lasing of current injected InGaN QD VCSELs covering most of the green region was achieved for the first time. This can mainly be attributed to the utilizing of high quality InGaN QDs as active region. The QDs showed strong carrier localization and negligible QCSE when compared with QW structure. The low threshold lasing in the "green gap" also benefitted from the good coupling between the QD layers and the electric field of the optical modes. The lasing wavelength can be controlled by adjusting the cavity length. These results open up opportunities to design and fabricate semiconductor green lasers with excellent performance that may lead to wide-gamut compact displays and projectors.

4. VCSELs based on QD-in-QW active structure

4.1. Properties of QD-in-QW structure

Using QD as the active layer material in a laser structure shows an escalating importance to the researchers for their latent significance in improving the device characteristics,[57] such as lowering threshold current.[56] This can be explained in terms of the QD's δ-function-like density of state. This has also been demonstrated in GaN-based green VCSELs as discussed in Sect. 3. However, the coverage of QDs on the sample surface is usually very small, and efficient carrier capture is hampered for a single layer of QDs. Designing multiple QD layers structure is proposed to provide sufficient carrier injection and gain for high injection efficiency and lasing. But too many layers may cause changes in QD shape and size, and finally the emission characteristics.[64] On the other hand, dot-in-well (QD-in-QW) structure has been proposed and widely used in GaAs-based light emitters[65,66] and lasers.[67,68] This section presents the first attempt at achieving dual wavelength lasing GaN VCSELs by using the QD-in-QW design.[20]

The VCSEL structure and the fabrication procedure is similar to VCSEL reported in previous section.[11] The active region uses a QD-in-QW design, with two pairs of $In_{0.27}Ga_{0.73}N$ (2.5 nm) QD layers embedded in $In_{0.1}Ga_{0.9}N$ (2 nm) QWs capped by an 8 nm thick GaN layer. We measured the SE spectra of the device without top DBR under different currents at RT, as shown in Fig. 4. The broad spectrum is observed owing to the inhomogeneity of the QDs in size and alloy composition.[69–71] We firstly observe a single broad peak at 525 nm under 100 μA, coming from the relaxation of carriers from high energy of the QW to the lowest energy state of QDs. As the current increases, the band filling effect in QDs[63] becomes dominant, which can explain why 525 nm emission peak is broadening at the shorter wavelength side. With the further increase of current, another sharp peak emitted from the QWs at 425 nm grows rapidly and becomes much stronger, because some localized carriers thermally escape from the QDs to QWs, and the carrier concentration increase in QWs. At even higher injection currents, the QDs become saturated and the recombination of carriers has mostly taken place in the QWs, thus the emission peak at 425 nm becomes pronounced. The energy separation between the two peaks is ~556 meV.

4.2. Emission spectra of VCSELs

The device exhibited dual wavelength lasing. Figures 5(a) and 5(c) show the lasing spectra of M1 and M2 under RT CW condition, respectively. The two lasing peaks is defined as M1 at 545 nm and M2 at 430 nm, respectively. It can be inferred from the EL spectra shown in Fig. 4 that the two lasing modes come from the emission of QDs and QWs, respectively. Figures 5(b) and 5(d) plots the peak emission intensities of the two lasing modes. The transition from spontaneous emission (SE) to stimulated emission can be observed clearly from the nonlinearly *L–I* (light–current) curve. A rapid narrowing of the linewidth with the injection current above the threshold is observed. These nonlinear curves are favorable evidence that stimulated emission appears. The threshold currents were of 2 μA for M1 which is the lowest value reported to date for GaN-based VCSELs. But this value is not precise because the distribution of current was not uniform when the injection current is low, especially the density of carriers flowing through the activated QDs should be much higher than the surrounding material. The true threshold current density may be relatively high in QDs. Therefore, such a low threshold current cannot reflect the true threshold current density in QD. And the threshold current for M2 is 5 mA.

CW operation of electrically pumped GaN-based VCSELs with simultaneous lasing in blue and green were realized by using QD-in-QW active region. In the QD-in-QW structure, the QDs can enhance the emission efficiency of the active layer due to the strong quantum confinement effect or carrier localization while the QW acts as a reservoir of carriers resulting in a higher capturing rate of carrier. These results open novel opportunities to design and fabricate multicolor

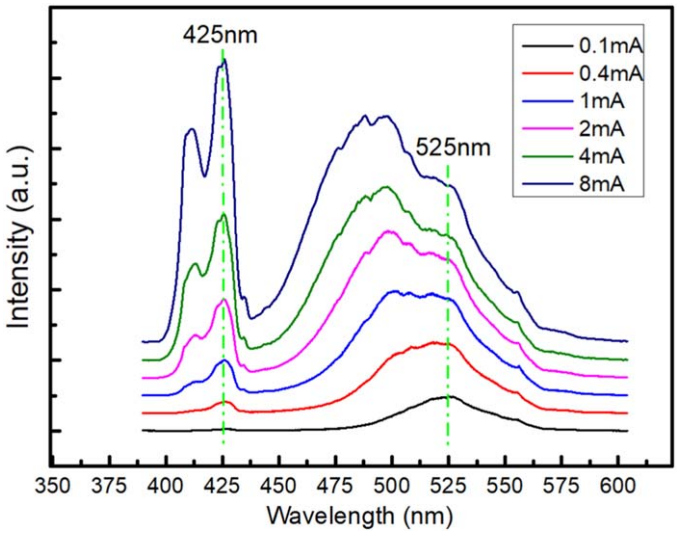

Fig. 4. (Color online) Electroluminescent (EL) spectra of the device without top DBR.

semiconductor laser sources, such as optical disk writing and reading, optical displays.

5. Green VCSELs based on purcell effect and localized states in QWs

5.1. Purcell effect

Microcavity lasers can realize an extremely high efficiency and high speed due to the volume effect and the control of SE. And the SE rate will be enhanced in a microcavity with a high quality factor (Q) and a small mode volume V, that a phenomenon known as the Purcell effect.[72,73] This is also called cavity effect. Benefit from the enhanced spontaneous emission, the carriers recombine much faster and the non-radiative Shockley–Read processes will have less impact. The Purcell factor (P) is controlled by the volume (V) and quality factor (Q) of the optical modes to which it is coupled,[74] and the P is given by:

$$P = \frac{3}{4\pi^2}\left(\frac{\lambda}{n}\right)^3 \frac{Q}{V},$$

where λ and n are the wavelength in the material and refractive index, respectively. Various microcavity devices could potentially display the Purcell effect, such as microdisks[75,76] and VCSELs.[76,77] For self-assembled InAs/GaAs quantum boxes, GaAs-based pillar microcavities and microdisks have large spontaneous emission factors of 5 and 15, respectively.[77] In case of a silicon-vacancy center in diamond embedded within a monolithic optical cavity, 10-fold lifetime reduction and 42-fold enhancement in emission intensity was observed when the cavity is tuned into resonance with the optical transition of the vacancy.[77] In this section, green VCSELs using a normally blue-emitting QWs are demonstrated. Lasing realized at the emission edge of the QWs is ascribed to the indium rich localization centers with combination of the cavity effect.[11]

5.2. Properties of cavity-induced green VCSELs

The cross section of the fabricated GaN-based VCSEL is similar with Fig. 2(a), with difference in DBR and active region. The device is featured with double dielectric DBR structure with a 13.5-pair Ti_3O_5/SiO_2 DBR and an 11-pair Ti_3O_5/SiO_2 DBR, served as bottom mirror and top mirror, respectively. The InGaN/GaN QW active region consisted of two periods of a 2.5 nm $In_{0.18}Ga_{0.82}N$ QW and a 6 nm GaN barrier. The fabrication procedure was similar with that described in Refs. 19 and, 20 with substrate transfer technique and laser lift-off process.

Figure 6 presents the RT electroluminescence (EL) spectra with different injection currents. The emission of cavity modes with on-resonance wavelengths are strongly enhanced with a resonant cavity. The cavity modes are divided into two groups MS1and MS2. MS1 is defined as laser mode from 433 to 457 nm, while MS2 is defined as laser mode from 475 to 505 nm. The intensity of the cavity modes at the boundary of MS1/MS2 is weak due to the smaller gain enhancement factor, or the weak coupling between active region and the antinode of the standing wave.[78] MS1 originates from the 2D QWs, while MS2 originates from InN-rich low-bandgap localization centers.[11] Carriers in the QW can be easily captured by the localization centers since they can freely move in the well-plane. At 20 mA, the intensity of MS1 is equivalent to that of MS2 as Fig. 6(a) showing. Under this current, the main mode in MS1 (439 nm mode) is stronger than that in MS2 (493 nm mode). Considering the low density of localized centers, it can be easily understood that more carriers recombine in QWs. With increasing current, localization centers in QWs capture much more carriers. The purcell effect can help to reduce the carrier lifetime and increase emission rate. The smaller lifetime means a higher radiative recombination efficiency. The emission from the localization centers shows a much faster growth rate. MS2 becomes stronger than MS1 with current increasing as Fig. 6(b) showing. Eventually, lasing at near green range (493 nm) was achieved when current is reaching threshold. Figures 6(c) and 6(d) show EL spectra when current is above threshold. The inset picture at (b) and (c) show nearfield patterns for device. These images were taken under low-gain settings to avoid saturating the camera. The green light is obviously observed within the current aperture, which can be attribute to Purcell effect. The leakage light from the circular DBR edge, which is due to SE without the Purcell effect, is always blue.

Figure 7 shows I–L and I–V characteristics of the VCSEL with a 15 μm diameter current aperture under CW operation

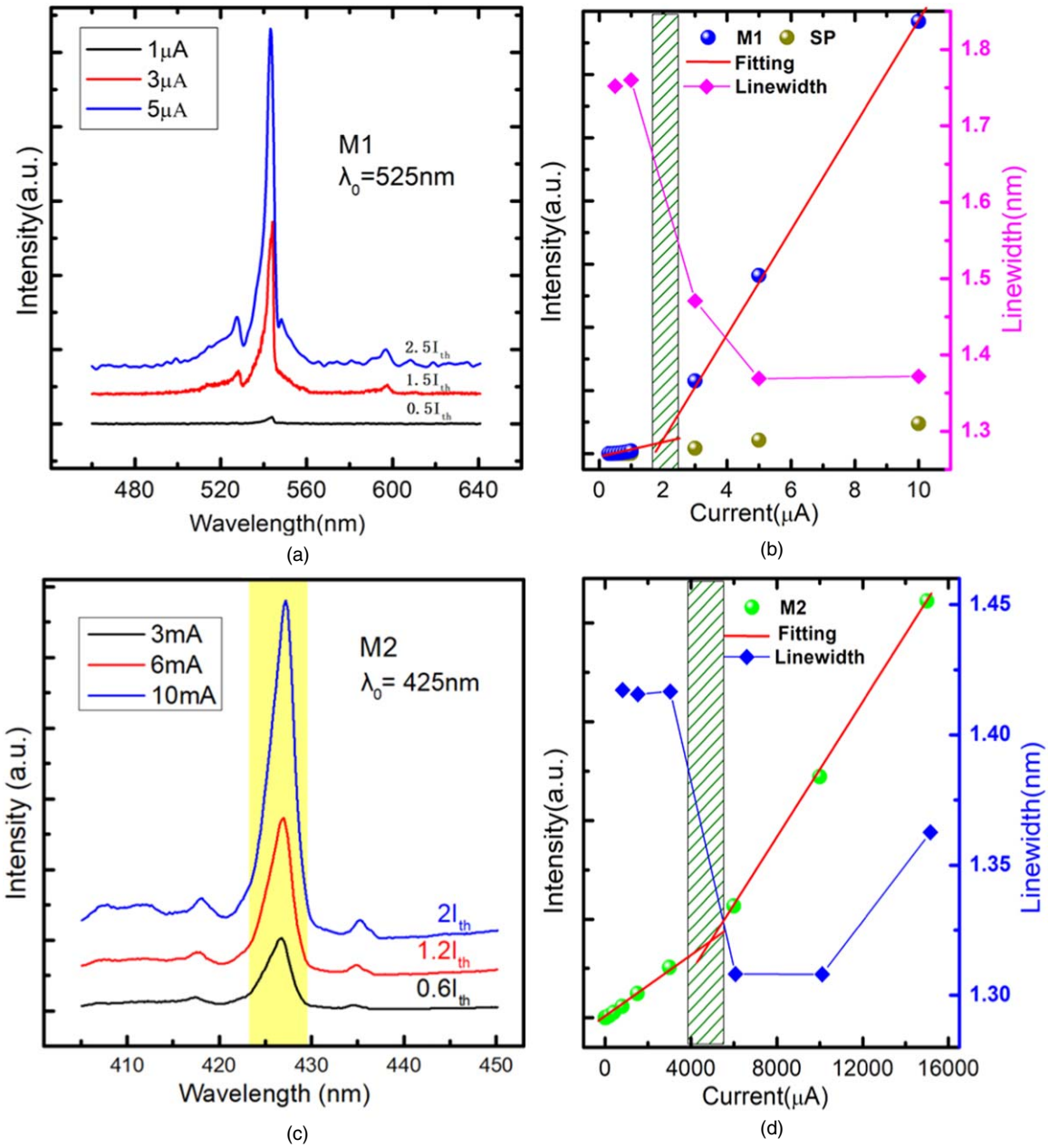

Fig. 5. (Color online) M1 (a) and M2 (c) laser emission spectra at various injection currents measured at RT. (b) Intensity and linewidth of M1 with corresponding spontaneous (SP) back ground as a function of current. (d) Intensity and linewidth of M2 as a function of current.

at 300 K. The *L–I* curve shows a clear kink at 32 mA, corresponding a threshold current density of 18 kA cm^{-2}. The output power of the device at 50 mA was ~178 μW. The degree of polarization of 71% under CW operation of 1.09 I_{th} is another evidence of lasing action (not given here). The different gain enhancement factor (Γ_r) can explain why the 493 nm mode achieve lasing. rather than the peak of the EL emission band (446 nm). Γ_r reflects the spatial overlap or coupling between the cavity mode and the emitting center and is given by:

$$\Gamma_r = \frac{L\int_{d_a}|E(z)|^2dz}{d_a\int_{L}|E(z)|^2dz},$$

where L, d_a, $E(z)$ are the cavity length, thickness of the active region and the electric component of the optical field standing-wave, respectively. The Γ_r has a crucial effect on the lasing characteristics such as threshold current density, which is deeply influenced by Γ_r. The threshold current density increases exponentially with Γ_r reduction when Γ_r is smaller than 1.[78)]

Figure 8 shows the optical field (squared electric field) of the 446 and 493 nm cavity modes calculated by the transfer matrix method. It is evident that 493 nm cavity mode shows a better coupling between the active region and the antinode of the optical field than 446 nm mode. The Γ_r is estimated to be 1.82 for 493 nm and 0.21 for 446 nm. Moreover, the longer lasing wavelength also benefits from less absorption loss in the active region.[79)]

The green GaN-based VCSELs using a normally blue-emitting QWs with a microcavity were realized. The green light originates from InN-rich lower bandgap localization centers at the emission edge of the QW. Owing to the cavity effect, the cavity-modes matched to localization centers are

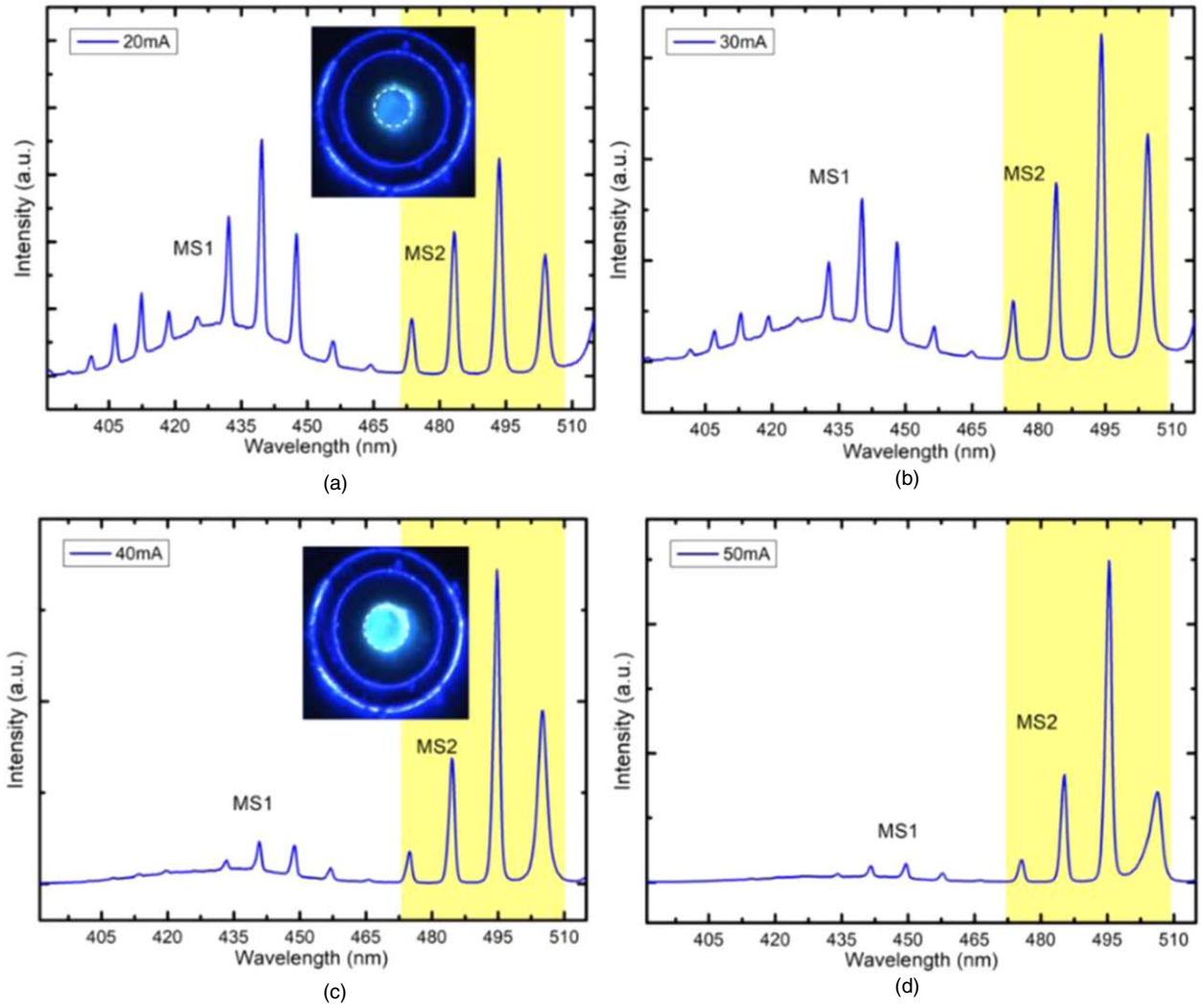

Fig. 6. (Color online) EL spectra of the VCSEL measured at four different currents (a) 20 mA (b) 30 mA (c) 40 mA (d) 50 mA. The inset picture shows nearfield patterns for device at (b) 20 and (c) 40 mA, respectively.

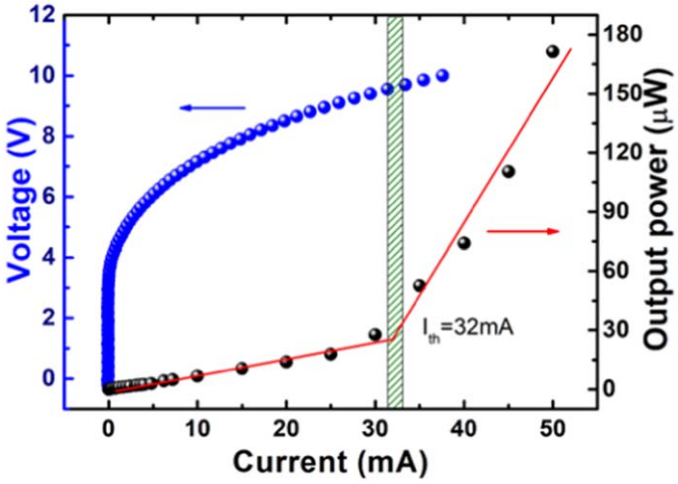

Fig. 7. (Color online) *I–L* and *I–V* characteristics of the VCSEL with a 15 μm diameter current aperture under. CW operation at 300 K.

strongly enhanced. With a larger gain enhancement factor and less absorption loss in the active region, lasing at green area is achieved. The result presents novel opportunities for the design and fabrication of green VCSELs. From the academic point, this method depends on the coupling between cavity modes and localization centers. Purcell effect plays an important role. From the application point, it allows QW with lower In content to reach VCSEL emitting longer

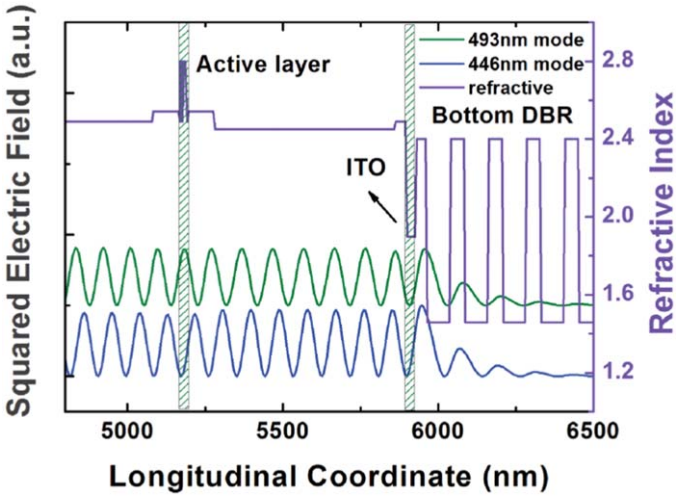

Fig. 8. (Color online) Refractive index and the distribution of the optical field for the 446 and 493 nm cavity modes of the VCSEL.

wavelength. However, there is still a lot of work to be done when considering the practical applications.

6. Summary

This paper discussed approaches toward GaN-based green VCSELs. In the commonly used QW active structure, there are few problems causing low emission efficiency, represented by the "green gap," such as defects, piezoelectric field, higher transparent carrier concentration, that make the realization of lasing difficult. However, QD active structure is highly expected to overcome these problems. Indeed, InGaN QD-based VCSELs have been demonstrated RT CW lasing with very low threshold currents and wavelengths of 479– 565 nm, coving most of the "green gap." By employing QD-in-QW active structure, the carrier capture efficiency can be increased and the threshold current be lowered further. Interestingly, dual-wavelength lasing, from QDs in the green and QWs in the blue, has been demonstrated. Another method to reach green lasing may be realized by using localization states, in a traditional blue-emitting QW with the help of a resonant cavity. The Purcell effect of a cavity is known to increase significantly the emission efficiency of a radiative center when resonance is achieved. It is also expected to enhance the recombination efficiency of the localization state in the QW, and at higher injections, lasing is obtained with QW as a reservoir for carrier supplier. When the emission of the localization center is in the green region, green VCSEL becomes possible. Based on this effect, VCSEL lasing at 493 nm has been demonstrated and an output power of 178 μW has been obtained.

Acknowledgments

We would like to show our sincere acknowledgements to Profs. Guo-En Weng, Hao Long, Zhi-Wei Zheng, Hao-Chung Kuo and Werner Hofmann for their help and useful discussions. This work was supported partially by the Science Challenge Project (No. TZ2016003) and partially by the National Key Research and Development Program of China (Nos. 2016YFB0400803, 2017YFE0131500).

1) H. Bazyar, M. Aghaie, M. H. Daemi, and S. M. Bagherzadeh, Opt. Laser Technol. **47**, 237 (2013).
2) R. Ashman, F. Reinholz, and R. Eikelboom, Lasers Med. Sci. **16**, 52 (2001).
3) P. Vieira, A. Manivannan, P. F. Sharp, and J. V. Forrester, Physiol. Meas. **23**, 1 (2001).
4) M. J. van Gemert and A. Welch, IEEE Eng. Med. Biol. Mag. **8**, 10 (1989).
5) N. J. Barber and G. H. Muir, Curr. Opin. Urol. **14**, 21 (2004).
6) J. S. Sandhu, C. Ng, B. A. Vanderbrink, C. Egan, S. A. Kaplan, and A. E. Te, Urology **64**, 1155 (2004).
7) H. M. Oubei, C. Li, K.-H. Park, T. K. Ng, M.-S. Alouini, and B. S. Ooi, Opt. Express **23**, 20743 (2015).
8) J. Xu, A. Lin, X. Yu, Y. Song, M. Kong, F. Qu, J. Han, W. Jia, and N. Deng, IEEE Photonics Technol. Lett. **28**, 2133 (2016).
9) Y. Chen, M. Kong, T. Ali, J. Wang, R. Sarwar, J. Han, C. Guo, B. Sun, N. Deng, and J. Xu, Opt. Express **25**, 14760 (2017).
10) X. Liu, S. Yi, X. Zhou, Z. Fang, Z.-J. Qiu, L. Hu, C. Cong, L. Zheng, R. Liu, and P. Tian, Opt. Express **25**, 27937 (2017).
11) R. Xu, Y. Mei, H. Xu, L. Y. Ying, Z. Zheng, H. Long, D. Zhang, B. Zhang, and J. Liu, IEEE Trans. Electron Devices **65**, 4401 (2018).
12) D. Kray, A. Fell, S. Hopman, K. Mayer, G. P. Willeke, and S. W. Glunz, Appl. Phys. A **93**, 99 (2008).
13) S. Engler, R. Ramsayer, and R. Poprawe, Phys. Proc. **12**, 339 (2011).
14) Y. Gan, Y. Lu, Q. Xu, and C.-Q. Xu, IEEE Photonics Technol. Lett. **25**, 75 (2012).
15) T. Mizushima, H. Furuya, K. Mizuuchi, T. Yokoyama, A. Morikawa, K. Kasazumi, T. Itoh, A. Kurozuka, K. Yamamoto, and S. Kadowaki, SID Symp. Digest of Technical Papers, 2006, p. 1681.
16) L. E. Cai, J. Y. Zhang, B. P. Zhang, S. Q. Li, D. X. Wang, J. Z. Shang, F. Lin, K. C. Lin, J. Z. Yu, and Q. M. Wang, Electron. Lett. **44**, 972 (2008).
17) D. Kasahara, D. Morita, T. Kosugi, K. Nakagawa, J. Kawamata, Y. Higuchi, H. Matsumura, and T. Mukai, Appl. Phys. Express **4**, 072103 (2011).
18) G. Weng, Y. Mei, J. Liu, W. Hofmann, L. Ying, J. Zhang, Y. Bu, Z. Li, H. Yang, and B. Zhang, Opt. Express **24**, 15546 (2016).
19) Y. Mei, G. E. Weng, B. P. Zhang, J. P. Liu, W. Hofmann, L. Y. Ying, J. Y. Zhang, Z. C. Li, H. Yang, and H. C. Kuo, Light: Sci. Appl. **6**, e16199 (2017).
20) R. B. Xu, Y. Mei, B. P. Zhang, L. Y. Ying, Z. W. Zheng, W. Hofmann, J. P. Liu, H. Yang, M. Li, and J. Zhang, Semicond. Sci. Technol. **32**, 105012 (2017).
21) D. Queren, A. Avramescu, G. Brüderl, A. Breidenassel, M. Schillgalies, S. Lutgen, and U. Strauß, Appl. Phys. Lett. **94**, 081119 (2009).
22) S. Yamamoto, Y. Zhao, C.-C. Pan, R. B. Chung, K. Fujito, J. Sonoda, S. P. DenBaars, and S. Nakamura, Appl. Phys. Express **3**, 122102 (2010).
23) M. Adachi et al., Appl. Phys. Express **3**, 121001 (2010).
24) Y. Enya et al., Appl. Phys. Express **2**, 082101 (2009).
25) K. Okamoto, J. Kashiwagi, T. Tanaka, and M. Kubota, Appl. Phys. Lett. **94**, 071105 (2009).
26) Y. Yoshizumi et al., Appl. Phys. Express **2**, 092101 (2009).
27) T. Kozaki, H. Matsumura, Y. Sugimoto, S.-I. Nagahama, and T. Mukai, Novel In-Plane Semiconductor Lasers V, 2006, p. 613306.

28) T. Miyoshi, S. Masui, T. Okada, T. Yanamoto, T. Kozaki, S.-I. Nagahama, and T. Mukai, Appl. Phys. Express **2**, 062201 (2009).
29) S. A. Veldhuis, P. P. Boix, N. Yantara, M. Li, T. C. Sum, N. Mathews, and S. G. Mhaisalkar, Adv. Mater. **28**, 6804 (2016).
30) M. S. Alias, Z. Liu, A. Al-Atawi, T. K. Ng, T. Wu, and B. S. Ooi, Opt. Lett. **42**, 3618 (2017).
31) S. Chen, C. Zhang, J. Lee, J. Han, and A. Nurmikko, Adv. Mater. **29**, 1604781 (2017).
32) Y. Wang, X. Li, V. Nalla, H. Zeng, and H. Sun, Adv. Funct. Mater. **27**, 1605088 (2017).
33) A. Meney, D. Prins, A. Phillips, J. Sly, E. O'Reilly, D. Dunstan, A. Adams, and A. Valster, IEEE J. Sel. Top. Quantum Electron. **1**, 697 (1995).
34) B. P. Zhang, The 24th Microoptics Conf. (MOC-2019), F-6 (Toyama, Japan), 2019.
35) S. Fujita, Japan. J. Appl. Phys. **54**, 030101 (2015).
36) J. S. Im, H. Kollmer, J. Off, A. Sohmer, F. Scholz, and A. Hangleiter, Phys. Rev. B **57**, R9435 (1998).
37) F. Della Sala, A. Di Carlo, P. Lugli, F. Bernardini, V. Fiorentini, R. Scholz, and J.-M. Jancu, Appl. Phys. Lett. **74**, 2002 (1999).
38) T. Langer, A. Kruse, F. A. Ketzer, A. Schwiegel, L. Hoffmann, H. Jönen, H. Bremers, U. Rossow, and A. Hangleiter, Phys. Status Solidi C **8**, 2170 (2011).
39) S. Nakamura, M. Senoh, N. Iwasa, and S.-I. Nagahama, Jpn. J. Appl. Phys. **34**, L797 (1995).
40) M. R. Krames, O. B. Shchekin, R. Mueller-Mach, G. O. Mueller, L. Zhou, G. Harbers, and M. G. Craford, J. Disp. Technol. **3**, 160 (2007).
41) J. Piprek, Phys. Status Solidi A **207**, 2217 (2010).
42) A. Laubsch, M. Sabathil, W. Bergbauer, M. Strassburg, H. Lugauer, M. Peter, S. Lutgen, N. Linder, K. Streubel, and J. Hader, Phys. Status Solidi C **6**, S913 (2009).
43) R. Singh, D. Doppalapudi, T. Moustakas, and L. Romano, Appl. Phys. Lett. **70**, 1089 (1997).
44) H. Zhao, R. A. Arif, and N. Tansu, J. Appl. Phys. **104**, 043104 (2008).
45) S.-H. Park, D. Ahn, and J.-W. Kim, Appl. Phys. Lett. **94**, 041109 (2009).
46) Z. Yang, R. Li, Q. Wei, T. Yu, Y. Zhang, W. Chen, and X. Hu, Appl. Phys. Lett. **94**, 061120 (2009).
47) Z. Deng, Y. Jiang, Z. Ma, W. Wang, H. Jia, J. Zhou, and H. Chen, Sci. Rep. **3**, 3389 (2013).
48) C. Du, Z. Ma, J. Zhou, T. Lu, Y. Jiang, P. Zuo, H. Jia, and H. Chen, Appl. Phys. Lett. **105**, 071108 (2014).
49) S. Saito, R. Hashimoto, J. Hwang, and S. Nunoue, Appl. Phys. Express **6**, 111004 (2013).
50) T. Miyoshi, S. Masui, T. Okada, T. Yanamoto, T. Kozaki, S.-I. Nagahama, and T. Mukai, Appl. Phys. Express **2**, 062201 (2009).
51) D. Bimberg, M. Grundmann, and N. N. Ledentsov, *Quantum Dot Heterostructures* (Wiley, New York, 1999).
52) L. Asryan and R. Suris, Semicond. Sci. Technol. **11**, 554 (1996).
53) C. Adelmann, J. Simon, G. Feuillet, N. Pelekanos, B. Daudin, and G. Fishman, Appl. Phys. Lett. **76**, 1570 (2000).
54) S. Lester, F. Ponce, M. Craford, and D. Steigerwald, Appl. Phys. Lett. **66**, 1249 (1995).
55) S. Schulz and E. O'Reilly, Phys. Rev. B **82**, 033411 (2010).
56) R. Tao and Y. Arakawa, Jpn. J. Appl. Phys. **58**, SCCC31 (2019).
57) M. Humayun, M. Rashid, and M. A. Malek, Indonesian J. Electr. Eng. Informatics (IJEEI) **7**, 441 (2019).
58) T. Newell, D. Bossert, A. Stintz, B. Fuchs, K. Malloy, and L. Lester, IEEE Photonics Technol. Lett. **11**, 1527 (1999).
59) P. G. Eliseev, A. A. Ukhanov, A. Stintz, and K. J. Malloy, 10th Int. Symp. on Nanostructures Physics and Technology, 2003, p. 350.
60) M. Asada, Y. Miyamoto, and Y. Suematsu, IEEE J. Quantum Electron. **22**, 1915 (1986).
61) Y.-R. Wu, Y.-Y. Lin, H.-H. Huang, and J. Singh, J. Appl. Phys. **105**, 013117 (2009).
62) Z. Li, J. Liu, M. Feng, K. Zhou, S. Zhang, H. Wang, D. Li, L. Zhang, Q. Sun, and D. Jiang, J. Appl. Phys. **114**, 093105 (2013).
63) G. E. Weng, W. R. Zhao, S. Q. Chen, H. Akiyama, Z. C. Li, J. P. Liu, and B. P. Zhang, Nanoscale Res. Lett. **10**, 31 (2015).
64) F. Heinrichsdorff, M.-H. Mao, N. Kirstaedter, A. Krost, D. Bimberg, A. Kosogov, and P. Werner, Appl. Phys. Lett. **71**, 22 (1997).
65) V. Ustinov, N. Maleev, A. Zhukov, A. Kovsh, A. Y. Egorov, A. Lunev, B. Volovik, I. Krestnikov, Y. G. Musikhin, and N. Bert, Appl. Phys. Lett. **74**, 2815 (1999).
66) S. Ray, K. Groom, M. Beattie, H. Liu, M. Hopkinson, and R. Hogg, IEEE Photonics Technol. Lett. **18**, 58 (2005).
67) L. Lester, A. Stintz, H. Li, T. Newell, E. Pease, B. Fuchs, and K. Malloy, IEEE Photonics Technol. Lett. **11**, 931 (1999).
68) G. Liu, A. Stintz, H. Li, K. Malloy, and L. Lester, Electron. Lett **35**, 1163 (1999).
69) L. Li, M. Rossetti, A. Fiore, L. Occhi, and C. Velez, Electron. Lett **41**, 41 (2005).
70) A. Kovsh, I. Krestnikov, D. Livshits, S. Mikhrin, J. Weimert, and A. Zhukov, Opt. Lett. **32**, 793 (2007).
71) K. A. Fedorova, M. A. Cataluna, I. Krestnikov, D. Livshits, and E. U. Rafailov, Opt. Express **18**, 19438 (2010).
72) E. M. Purcell, H. C. Torrey, and R. V. Pound, Phys. Rev. **69**, 37 (1946).
73) E. M. Purcell, *Confined Electrons and Photons* (Springer, Berlin, 1995), p. 839.
74) K. Ujihara, Jpn. J. Appl. Phys. **30**, L901 (1991).
75) B. Gayral and J. Gerard, Physica E **7**, 641 (2000).
76) D. Deppe and H. Huang, Appl. Phys. Lett. **75**, 3455 (1999).
77) Y. T. He, X. Y. Lei, Z. R. Qiu, B. P. Zhang, N. Lu, I. T. Ferguson, and Z. C. Feng, Appl. Mech. Mater. 187 (2014).
78) Y. Mei, R.-B. Xu, G.-E. Weng, H. Xu, L.-Y. Ying, Z.-W. Zheng, H. Long, B.-P. Zhang, W. Hofmann, and J.-P. Liu, Appl. Phys. Lett. **111**, 121107 (2017).
79) C. A. Forman, S. Lee, E. C. Young, J. A. Kearns, D. A. Cohen, J. T. Leonard, T. Margalith, S. P. DenBaars, and S. Nakamura, Appl. Phys. Lett. **112**, 111106 (2018).